JOURNAL OF PROPULSION AND POWER
Vol. 13, No. 6, November–December 1997

Assessment of Jet Noise Analysis Codes for Multistream Axisymmetric and Forced Mixer Nozzles

T. J. Barber* and L. M. Chiappetta†
United Technologies Research Center, East Hartford, Connecticut 06108
and
S. H. Zysman‡
Pratt and Whitney, East Hartford, Connecticut 06108

Jet noise effects produced by an axisymmetric multistream exhaust nozzle have been examined using computational and experimental techniques. The current approach for designing low noise exhaust systems uses empirical rules and computational fluid dynamics (CFD) calculations aimed at lowering peak velocities and/or temperatures. Engineers need to be able to predict noise directly and use predictions to support their specific design goals. The computational approach utilized in this paper applies a state-of-the-art CFD Navier–Stokes analysis (NASTAR), in conjunction with a computationally based aeroacoustics analysis. The aeroacoustic analysis uses mean flow properties and turbulent kinetic energy/dissipation variables as input parameters for the aeroacoustic solver. Predictions have been made and compared to experimental data obtained in NASA Lewis Research Center's open-jet facility. More specifically, comparisons of aerodynamic and acoustic parameters have been made for axisymmetric nozzles to identify the effects of turbulence level, compressibility, geometrical sizing, and forward flight on measured levels of jet noise. Applicability of this analysis approach to three-dimensional forced mixer configurations has also been explored, with a limited degree of success.

Nomenclature

A	=	area
a	=	speed of sound
BPR	=	bypass ratio, $m_{\text{bypass}}/m_{\text{core}}$
D	=	nozzle diameter
f	=	observed frequency
g	=	shielding function
k	=	turbulence kinetic energy
m	=	mass flow
P	=	pressure
R	=	distance to observer
r	=	radial coordinate
T	=	temperature
U	=	axial velocity component
V	=	vertical velocity component
x	=	axial coordinate
α, α_T, β_c	=	empirical constants
ε	=	turbulent dissipation
η	=	temperature mixedness
θ	=	viewing angle referred to upstream
ρ	=	density
τ	=	characteristic time delay
Ω	=	source frequency

Subscripts

b	=	bypass stream condition
c	=	convective reference
cl	=	centerline
fs	=	full or engine scale
j	=	jet exit plane condition
m	=	fully mixed outplane
p	=	primary stream condition
ss	=	small or model scale
x	=	axial location
0	=	stagnation condition
∞	=	freestream condition

Superscript

$'$	=	turbulent fluctuation

Presented as Paper 96-0750 at the AIAA 34th Aerospace Sciences Meeting, Reno, NV, Jan. 15–18, 1996; received July 22, 1996; revision received May 27, 1997; accepted for publication June 2, 1997.

*Manager. E-mail: bar@utrc.utc.com. Associate Fellow AIAA.
†Senior Research Engineer. E-mail: luey@utrc.utc.com. Senior Member AIAA.
‡Research Engineer. Member AIAA.

Introduction

FEDERAL Aviation Administration (FAA)-imposed stage 3 noise requirements will place strong operating restrictions on aircraft that are currently in use. In extreme cases, financial penalties may be imposed and some aircraft types may be banned from operating. A primary component of the measured noise during takeoff is jet noise, produced by the turbulent mixing of the engine flow with the ambient, or external, airstream. Since the late 1960s, internal forced mixing has been used extensively in low bypass ratio (LBPR) engines, such as Pratt and Whitney's family of JT8Ds, to obtain thrust augmentation, improved thrust-specific fuel consumption (TSFC), and noise reduction. Forced mixing combines the hot, or turbine, exit flow with the cold fan, or bypass, flow prior to acceleration of the flows through the exhaust nozzle. Internal mixers often use convoluted surfaces, shaped like a cookie-cutter, to form the annular dividing surface (between core and bypass flow) to achieve improved mixing (Fig. 1). Two driving mechanisms have been postulated to explain this long-observed phenomena: 1) the generation of large-scale streamwise vortices and 2) the generation of an increased shear-layer perimeter. Experimental parametric studies have also shown that improved mixing is frequently obtained at the expense of increased flow losses.

The design and development of internal mixers has until recently utilized cut and try techniques to optimize exhaust system performance. Complicating the design process is the observation that the forced mixer has many important scales,

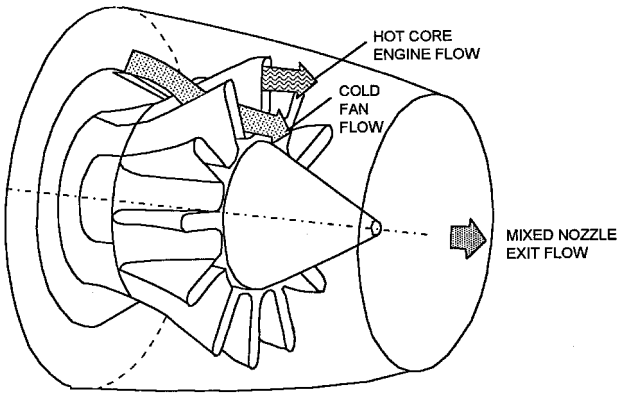

Fig. 1 Typical lobed forced mixer exhaust geometry.

e.g., the number of lobes, lobe height, lobe aspect ratio, lobe shape, etc. Because of the geometrical and physical complexity of the problem, computational fluid dynamics (CFD) techniques have traditionally had little impact on the design process, because of limitations from available 1) computational power, 2) grid generation techniques, and 3) reliable CFD solvers, as well as 4) the lack of a good understanding of the dominant flow mechanisms. As more powerful computers and improved computational methods have become available, CFD techniques have been applied in the design process.

Conventional design processes apply empirical rules and CFD analyses. A key design criterion of these analyses has been to reduce the peak levels of velocity and temperature at the nozzle exit plane. A general-purpose Navier–Stokes analysis[1] (NASTAR) has been applied in such a manner to design forced mixer/nozzle configurations. In one validation study,[2] a high-penetration 18-lobed mixer for the NASA-supported high-bypass ratio Energy Efficient Engine (E^3) was analyzed and the results were compared to experimental data.

The aim of the following research study is to determine if advanced CFD and computational aeroacoustics (CAA) and computational techniques can be used to provide a more direct analysis of the jet noise characteristics of advanced exhaust nozzle systems. The viscous flow analysis used in this study is the NASTAR code. Jet noise penalties are assessed from a variety of predicted flowfield-based parameters. Analytically based acoustic signature assessments are performed using NASA Lewis Research Center's (LeRC) modified version of the FAA Mani-Gliebe-Balsa (MGB) analysis.[3] This study will calibrate these analyses for axisymmetric multistream nozzles as well as assess the applicability of the analyses to three-dimensional forced mixer nozzles.

NASTAR Navier–Stokes Analysis

The viscous flow analysis used was the NASTAR code, which solves the Reynolds-averaged form of the governing equations for steady, three-dimensional flows, including the effects of turbulence and heat release caused by chemical reaction. The code is based on the method by Rhie and Chow.[1] Essentially, NASTAR represents a significant extension of the pressure-correction methodology used in the TEACH family of codes.[4] The governing equations are approximated using a finite volume method. The discretized continuity and momentum equations are used to derive a pressure-correction equation that is used in place of the continuity equation. Rhie and Chow's method[1] provides a single-cell, general curvilinear coordinate procedure that is applicable for Mach numbers ranging from incompressible flow to hypersonic flow. The results described in the current study were obtained using the two equation (k-ε) model for turbulence.[5]

The algorithm used in NASTAR provides for a controlled amount of numerical damping based on the local cell Reynolds number to promote numerical stability. Various measures were used to determine whether the computation was converged sufficiently. NASTAR evaluates residual errors as well as selected integral measures. These measures can be used to assess convergence characteristics, aerodynamic performance, and jet noise penalties, e.g., contours of stagnation temperature T_0 at the mixing duct/nozzle exit plane, profiles of axial velocity U downstream of the mixer and at the nozzle exit plane, and mixedness $\eta(x)$ defined as

$$\eta = 100\left(1.0 - \frac{\int \rho U|T_{0x} - T_{0m}|\,\mathrm{d}A}{\int \rho U|T_{0i} - T_{0m}|\,\mathrm{d}A}\right) \tag{1}$$

where the subscript i refers to the initial axial plane in the mixing duct. Experience shows that each nozzle case required approximately 5000 iterations to achieve convergence.

The primary measure for jet noise reduction, however, has been that lower jet noise corresponded to reduced peak velocity and temperature profiles at the exit plane of the exhaust nozzle. In the next section, we will consider a computationally based aeroacoustic (CBA) analysis aimed at directly predicting noise spectra [sound pressure level (SPL)] and acoustic signatures [overall sound pressure level (OASPL)].

MGB Acoustics Analysis

The direct computation of an engine exhaust sound field by solving the unsteady flow form of the Navier–Stokes equations (CAA) is currently not feasible. An alternative approach based on a unified aerodynamics/acoustics prediction analysis has been developed by Mani et al.[3] and is called the MGB analysis. Mani et al.[3] followed Lighthill's original assumption that the turbulent fluctuations produced in the mixing regions of the jet are the primary source of noise generation. The MGB solution technique is described in two sections: 1) source/spectrum modeling and 2) sound/flow interaction.

In the first part, the aerodynamic predictions from a flowfield analysis are used to model the source strength and its spectrum. In the original version, this analysis was based on the semiempirical Reichardt model. Khavaran et al.[6,7] developed an improved model that incorporates a steady-state Navier–Stokes analysis to determine the mean flow aerodynamics together with k and ε turbulence parameters to define the eddy scales. The acoustics solution applies Lighthill's acoustic analogy. The source terms in the acoustics equation are determined by applying Ribner's model (for which the correlation function is a linear combination of second-order tensors), assuming isotropic turbulence. While the original analysis applied Davies empirical model (based on the mean shear, $\partial U/\partial r$) for the turbulent eddy scales, the current analysis assumes a scaling based on k-ε, a turbulent time scale. The source and spectrum tensor I is proportional to $k^{7/2}$ and includes Doppler shift and convective Mach number effects. The Doppler effect provides a relationship between Ω and f.

Lighthill's acoustic analogy approach does not incorporate the effect of the surrounding mean flow on the sound radiated by convected multipole sources. Pressure fluctuations propagate through regions of nonuniform velocity and temperature before reaching the observer point. Thus, the location of the source within the jet determines the amount of radiated sound. The mean flow affects the refraction of the radiated sound and provides an additional convective amplification factor.

In the second part of the MGB analysis, Mani et al.'s[3] formulation for the sound/flow interaction for axisymmetric geometries is adopted; i.e., the turbulent properties of the jet are coupled with its acoustic radiation. The mean square pressure in the far field is an integrated effect of 1) a factor related to the source intensity and frequency and 2) a series of directivity factors, which are functions of the flow and convective Mach

numbers. Consistent with acoustical modeling practice, these Mach numbers are defined with reference to the freestream speed of sound. The acoustical signature or SPL for an axisymmetric jet is expressed in terms of the mean square pressure field

$$\mathrm{SPL} = 10 \log_{10}\left(\frac{\bar{p}^2}{p_{\mathrm{ref}}^2}\right) = 10 \log_{10}\left[\int \Lambda f(a_{ij})\, \mathrm{d}V\right] \quad (2)$$

where Λ is a factor related to the source intensity and frequency, and the a_{ij} are directivity factors expressed in terms of the polar observation angle θ, the local sound speed, and flight and convective Mach numbers through a shielding function. The mean square of the pressure field at a point in space, from all sources, can be approximately given as

$$\bar{p}^2 \approx \left(\frac{1}{4\pi R}\right)^2 \{(\omega\tau_0)^4 \exp[-(\Omega\tau_0)^2/8]\}(\rho_\infty^2 k^{7/2}\Delta V) \times \left[\frac{(1 - M\sin\theta)^4 a_\infty^6}{(1 - M_c \sin\theta)^2 a^6}\right]\left[\frac{1}{(1 + M_\infty \sin\theta)}\right]\beta \quad (3)$$

where the source intensity spectrum and flow shielding factors are defined as follows:

$$I(\Omega) \approx \rho_\infty k^{7/2}(\Omega\tau_0)^4 \Delta V \quad (4)$$

$$\beta = \exp\left[-2\left(\frac{\Omega}{a_\infty}\right)\int |g^2(r, \theta, M_c, M)|^{1/2}\, \mathrm{d}r\right] \quad (5)$$

and other key parameters are defined as follows:

$$M = \frac{U}{a_\infty}, \quad M_j = \frac{U_j}{a_\infty}, \quad M_c = 0.5(M - M_\infty) + \beta_c(M_j - M_\infty)$$

$$\tau_0 = \left(\frac{k}{\varepsilon}\right)\left(\frac{1}{\alpha}\right) = \text{characteristic time delay}$$

$$\Omega = 2\pi\omega\left[(1 - M_c \sin\theta)^2 + \alpha_T \frac{k^{1/2}}{a_\infty}\right]^{1/2}$$

The parameters α, α_T, and β_c are user-specified constants that are empirically determined. The angle θ is measured from the jet centerline starting from the inlet or upstream direction. More frequently, however, SPL is converted into a weighted average, such as OASPL. OASPL integrates SPL at a given measurement location/orientation over all frequencies.

Nozzle Geometry and Experimental Data

The experimental data cited in this study[8,9] were obtained in the Nozzle Acoustic Test Rig (NATR) at LeRC. The rig consists of a 53-in.-diam freejet situated in a 62-ft radius dome. The jet is capable of supplying nozzle pressure ratios up to 5.0 and jet stagnation temperatures of 2000°R. The current study focuses on an axisymmetric multistream nozzle flowfield, consisting of a hot primary inner flow, a cold secondary flow

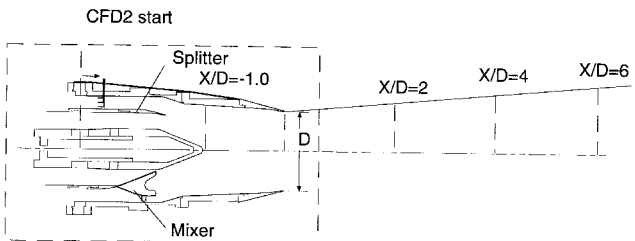

Fig. 2 Schematic of exhaust nozzle installations in NASA NATR test facility.

Table 1 NATR test conditions

M_∞	T_{0_p}, °R	T_{0_s}, °R	T_{0_∞}, °R	P_{0_p}, psi	P_{0_s}, psi	P_{0_∞}, psi
0.10	1442	542	533	28.02	26.43	14.30
0.27	1438	508	527	28.81	26.13	15.10

(separated from the primary by a splitter surface), and an external stream representing low-speed ambient takeoff conditions (Fig. 2). The overall length of the model has been designed to account for thermal growth effects. Figure 2 also illustrates the use of a wind-tunnel contraction section, designed to minimize the growth of the boundary layer over the external surface of the nozzle. Total pressure and temperature profiles were experimentally determined by probes located at the upstream charging station ($x/D = -11.6$). One-dimensional averages of these measurements are shown in Table 1. Figure 2 shows the location of laser Doppler velocimetry (LDV) traverses in terms of an axial coordinate referenced to the nozzle diameter. A single internal traverse plane was measured. Microphone arrays located 50 ft from the model measured spectra that have been processed in a one-third-octave format.

All acoustic data were taken to match the sideline takeoff acoustic condition ($M_\infty = 0.27$). All LDV data were taken at a high power point corresponding to a primary nozzle pressure ratio of about 2.0 and a freestream Mach number of 0.10. A higher Mach number was desired to match the sideline acoustic condition, but this was prevented by excessive vibration of the LDV system.

Computational Model

The calculations were performed in two stages. Initially, a calculation (CFD1) was completed from the upstream charging station to a station where the lobed mixer would begin in a three-dimensional flow case. The results of this calculation provided inlet profiles for all subsequent aerodynamic calculations. These latter calculations (CFD2) were performed from the mixer inlet station, through the nozzle exit plane, to a plane approximately 17 nozzle diameters downstream of the nozzle exit. The forced mixer calculations were performed on a computational domain that extended 12D downstream, with some axisymmetric calculations extending the domain to 20D. Based on an observation concerning the impact of turbulence level on the OASPL acoustical signature, parametric studies varying the inlet turbulence profile were conducted. Two types of calculations were performed. In the first type, levels of freestream turbulence and an improved wall boundary condition were imposed to achieve a best match with the measured downstream level of turbulence energy. This type of best calculation used a single-block Cartesian grid of 400 by 133 (53,200) points (Fig. 3). A second approach was also pursued, whereby the measured U' data were used to define a turbulent kinetic energy profile at the $x/D = -0.8$ station. A single-block Cartesian grid of 254 by 167 (42,418) points was used for these experimentally started calculations.

The generation of lobed mixer grids involved a multistep process: determination of the surface geometry, generation of two-dimensional slices at constant axial planes, generation of two-dimensional grids using an expert system, knowledge-based analysis,[10,11] and stacking of the two-dimensional grids to form a final three-dimensional grid. Single blocked-structured grids were generated with internal surfaces defined using cell types for the cells internal to solid sections that indicate no flow is present. This feature is a generalization of the IBLANK concept used in codes accepting grid files in PLOT3D format. Each case considered a half-lobe geometry, assuming symmetry planes in the azimuthal direction. A typical grid used about 185,000 points (71 axial, 75 radial, and 35 azimuthal). Specific cells on the lobe surface were identified as flow-through cells, creating a stair-step description of the scallop. Figure 4 illustrates a typical axial (crest-cut) and cross-sec-

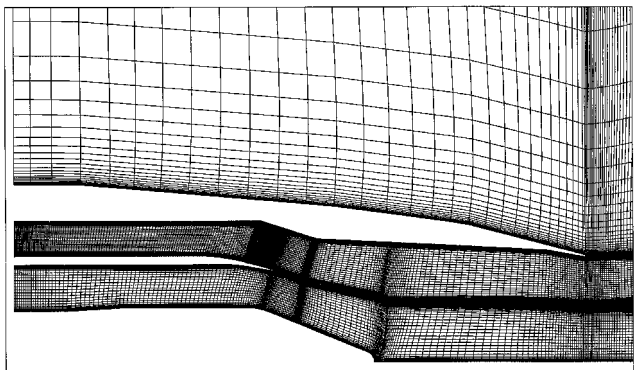

Fig. 3 Splitter configuration axial grids.

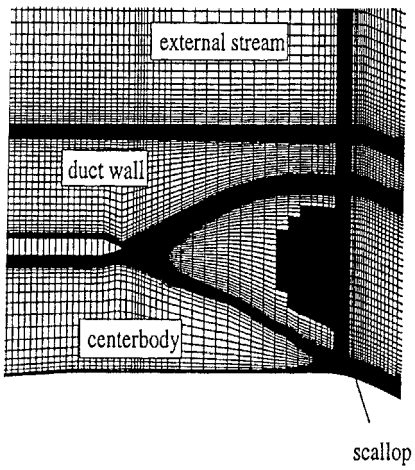

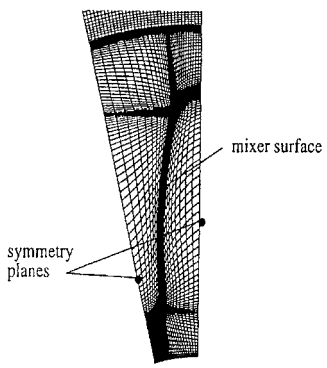

Fig. 4 Mixer configuration grids.

tional grid and the cells for modeling the effects of scalloping (cutouts) and scarfing (cutback) case. The axial extent of the computational domain was approximately 10 nozzle diameters downstream of the exit plane. The radial extent of the domain was five nozzle diameters.

Results of the flowfield calculations were presented in Ref. 9. These results confirmed that lobed-mixer nozzles have lower exit plane axial velocities than found in splitter (separating fan and primary flows) nozzles. Table 2 illustrates this in terms of an improved mixedness of the exit flow using a lobed mixer nozzle. Table 2 also illustrates the effect of increased mixedness with increased lobe number. All calculations cited in Table 2 were performed for the same operating point. In addition, the mixer calculations were made for mixers without scalloping.

Axisymmetric Splitter Studies

The splitter configuration cases are axisymmetric cases for which test data are available for model validation. Navier–Stokes calculations have been performed for a 17,000-lb thrust

Table 2 Calculated mixedness

Nozzle type	η, %
Splitter	11.9
12-lobed mixer	70.5
20-lobed mixer	74.9

case corresponding to sideline takeoff noise operation. Calculations were obtained for forward-flight conditions of M_∞ = 0.1, where aerodynamic (*LV*) data were obtained, and M_∞ = 0.27, corresponding to conditions where acoustical data were obtained. Converged solutions required approximately 6000 iterations.

Based on observed differences between the predicted k and the measured *LV* fluctuating velocity component U', V', parametric studies varying the inlet turbulence profile were conducted. Variations considered included increased levels of freestream turbulence and an improved near-wall boundary condition. Both of these modifications resulted in modestly improved levels of turbulence in the plume. An alternative strategy was also pursued, whereby the measured U' data were used to define a turbulent kinetic energy profile at the x/D = −0.8 station. The V' and W' components were defined at 0.7 of U' based on previous empirical data. The resultant calculations showed substantially improved agreement with the downstream *LV* data. Comparisons between computed and measured U and U', V' are shown in Ref. 8. Good agreement is noted for the mean axial velocity component. The NASTAR predictions show some slight undermixing relative to the measured data. Note that NASTAR assumes isotropic turbulence and predicts turbulent velocity components from k distribution. In addition, the experimental fluctuating velocity component data were obtained for only two of the three turbulent velocity components.

Based on these comparisons, parametric studies have been performed to investigate whether certain CFD modeling factors will have a major impact on any noise analysis calibrations.

Turbulence Initialization Issues

NASTAR comparisons of U', V' with *LV* measured data[8] have identified the effect of using different starting profiles for the turbulence variables. These comparisons were performed at the forward-flight condition of M_∞ = 0.1, where aerodynamic, not acoustic, data were measured. Comparisons of NASTAR–MGB predictions of OASPL for model-scale conditions operating at the LDV test point indicate an approximately 2–3 dB difference between the different initialization approaches (Fig. 5). Approximately 0.5 dB can be accounted for by comparing the peak values of k in the near-field shear layer, using

$$\text{SPL error} = 10 \log_{10}(k_{\text{exp profile}}/k_{\text{base profile}})^{7/2} \qquad (6)$$

As expected, the larger turbulence levels observed in the experiment produce the higher acoustic signature.

Compressibility Issues

Because the model for the generation of jet noise depends strongly on the computed turbulence intensity and dissipation rate, it is expected that the predicted acoustical signature is dependent on the turbulence model used by the Navier–Stokes solver. Of particular concern is whether compressibility effects have a strong influence on the MGB-predicted acoustical signature. It is important to note that when the convective (aerodynamic) Mach number approaches unity, the jet spreading rate decreases appreciably. The so-called Langley curve,[12] representing several planar shear-layer data sources, illustrates this effect. Recently, turbulence model sensitivity studies were performed using the new MGB code and United Technologies Research Center's Navier–Stokes code.[13] The test case was

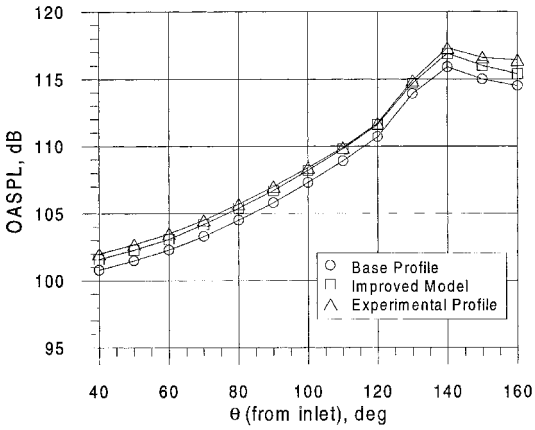

Fig. 5 Effect of inlet turbulence profile on OASPL.

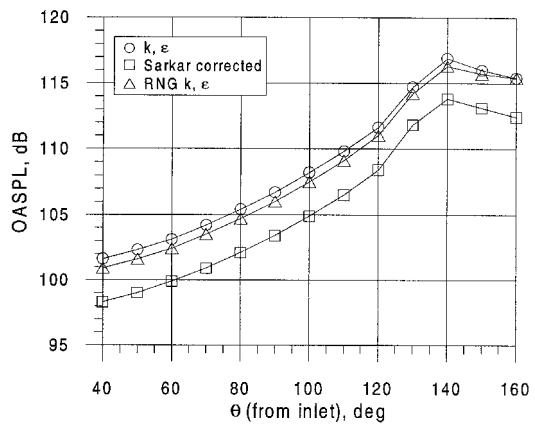

Fig. 6 Effect of turbulence model on OASPL.

Yamamoto et al.'s[14] underexpanded convergent nozzle (case 114). The Reynolds number of the jet, based on exit flow conditions and the nozzle diameter, is about 1.4×10^6; therefore, the flow can be considered fully turbulent. The effect of different turbulence models was evaluated for the standard k-ε model,[15] the compressibility corrected Sarkar k-ε model,[12] and the renormalization group (RNG) k-ε model.[15] Approximately 2-dB shift caused by compressibility effects was noted.

Defining an approximate convective Mach number for axisymmetric jet flows

$$M_c = \frac{(U_{cl} - U_\infty)}{(a_{cl} + a_\infty)} \tag{7}$$

the maximum value of M_c for Yamamoto et al.'s[14] case is about 0.78. At this level, the spreading rate is reduced from its incompressible value by about 30%. In the current splitter case, M_c is approximately 0.55 in the potential core and decreases downstream in the plume. Correspondingly, the centerline Mach number is barely sonic in the potential core and also decreases downstream in the plume. At this M_c level, the effect of compressibility reduces the jet spreading rate by less than 5%, and the standard k-ε model should be adequate for all splitter and lobed mixer cases as far as the compressibility effects are concerned.

Although compressibility effects should be expected to have little impact on the acoustic signature, Fig. 6 compares MGB predictions using assorted turbulence models in the NASTAR flow solver. The flowfield results indicate little difference in the near field of the jet; however, the predictions confirm results previously observed by Choi et al.,[15] where k-ε predictions mix out more rapidly, whereas using the Sarkar compressibility correction reduces the effective spreading rate. The mixing rate of hot jets can be significantly impacted by thermal diffusion effects ($Pr_t \neq 1$). All predictions cited in the text do not account for this effect.

MGB Calibration

Baseline acoustical predictions obtained using NASTAR and MGB for the 17,000-lb thrust case corresponding to sideline takeoff noise operation are shown in Figs. 7 and 8. Figures 7 and 8 show a comparison of the predicted OASPL and an aft-looking spectra for a model scale geometry at 50-ft arc distance. The OASPL levels, especially for the rearward-looking orientation (primary noise source), show good agreement with data. The effect of inlet turbulence profile does not appear to have a significant effect on the exhaust signature. The predicted spectra also show good agreement with measured peak levels; however, a predicted dip in the 20–25 band number range is not seen in the experimental data. This result was also observed in predictions using the NPARC Navier–Stokes analysis.[16]

Model-to-Engine Scaling

A majority of jet noise data, as in this program, have been acquired at small scale. Full-scale or engine-size data are typically extrapolated from the small-scale databases. When jet

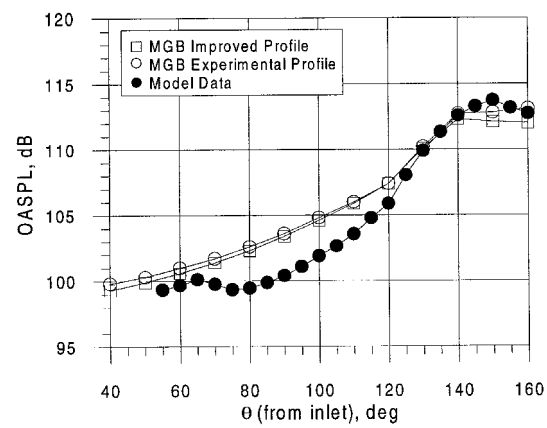

Fig. 7 Model scale splitter OASPL comparisons at 50-ft distance.

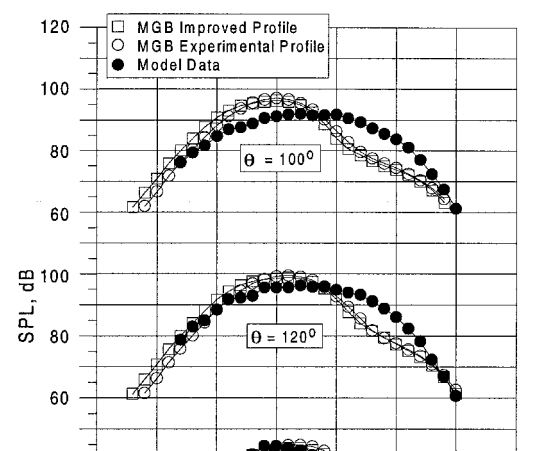

Fig. 8 Model scale splitter one-third octave spectra comparisons at 50-ft distance.

noise mechanisms are dominant, semiempirical equations are used. By assuming equal jet velocity, temperature, and environmental conditions, corrections can be made for jet size, observer distance, and acoustic frequency,[17] i.e.,

$$\mathrm{SPL_{fs}} - \mathrm{SPL_{ss}} = 10\log_{10}\left(\frac{D_{\mathrm{fs}}}{D_{\mathrm{ss}}}\right)^2 - 10\log_{10}\left(\frac{R_{\mathrm{fs}}}{R_{\mathrm{ss}}}\right)^2 + 10\log_{10}\left(\frac{\Delta f_{\mathrm{fs}}}{\Delta f_{\mathrm{ss}}}\right) \tag{8}$$

The first term in Eq. (8) is based on the assumption that acoustic power increases directly with the source area. The second term relates acoustic power decay to an inverse-square law. The third term, a correction for filter bandwidth, assuming the data were acquired in third-octave bands, is not always used. Manifest in this equation is the assumption that the same physical phenomena that are dominant at large scale are also dominant at small scale. For example, the scaling of jet frequencies is based on the observation that the dominant large-scale turbulence-induced noise occurs at constant Strouhal number ($St = fD/U_j$), even for a large range of Reynolds numbers. Thus, the frequency shift with scale for equal velocity jets can be expressed as follows:

$$f_{\mathrm{fs}} = f_{\mathrm{ss}}\frac{(StU_j/D)_{\mathrm{fs}}}{(StU_j/D)_{\mathrm{ss}}} = f_{\mathrm{ss}}\left[\frac{D_{\mathrm{ss}}}{D_{\mathrm{fs}}}\right] \tag{9}$$

Therefore, by keeping the acoustic wavelength to jet diameter ratio constant, jet noise directivity patterns are assumed to be maintained.

Scaling studies have been performed using NASTAR and MGB for a configuration at 17,000-lb thrust, corresponding to the sideline takeoff noise operation point. Three calculations were performed to compare with the measured data: 1) a model-scaled CFD and MGB calculation, 2) a model-scaled CFD and an engine-scaled MGB, and 3) a full-size (engine) CFD calculation with its corresponding MGB calculation. The model-scale calculations were evaluated at 50-ft arc distance. These calculations were also scaled to full-scale engine conditions at a 150-ft arc distance. The last calculation was a CFD analysis of a full-scale engine nozzle evaluated at 150-ft distance. In the second analysis, the flowfield was assumed to be unchanged (no Reynolds number effect), so that the geometry could be directly scaled by a factor of 7.0, the ratio of full-scale to model-scale size. The model test data were also rescaled to engine size at 150-ft distance using a NASA LeRC procedure. Figures 9 and 10 illustrate the comparison. The CFD results indicate little *Re* effect in the rescaling calculations (about 1 dB). Also note from the spectra results of Fig. 10 the expected spectra shift to lower frequencies (band numbers) with increased configuration size.

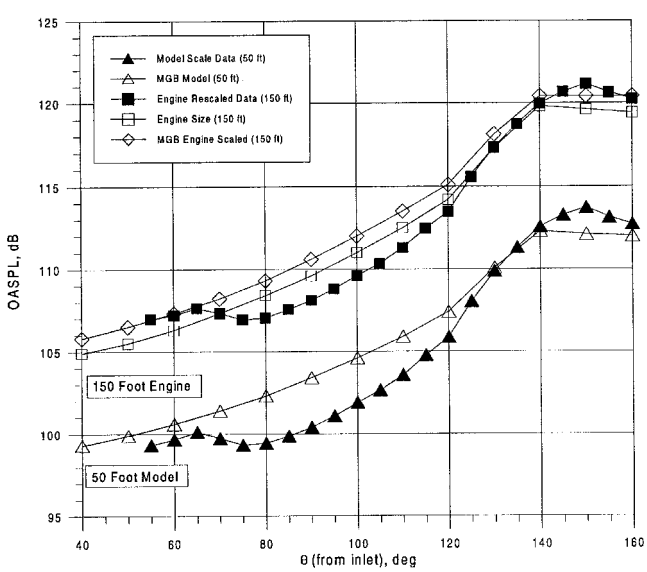

Fig. 9 Engine scaled splitter OASPL comparisons at 150-ft distance.

Forward-Flight Effects

Extensive data in the open literature have demonstrated that a reduced flight velocity results in an increased acoustical signature. Acoustic data taken at the $M_\infty = 0.27$ and at a static or no forward-flight condition confirm this observation. Flowfield calculations for these conditions were attempted; however, numerical instabilities at the static condition were encountered. Instead, flow calculations were obtained for the forward-flight

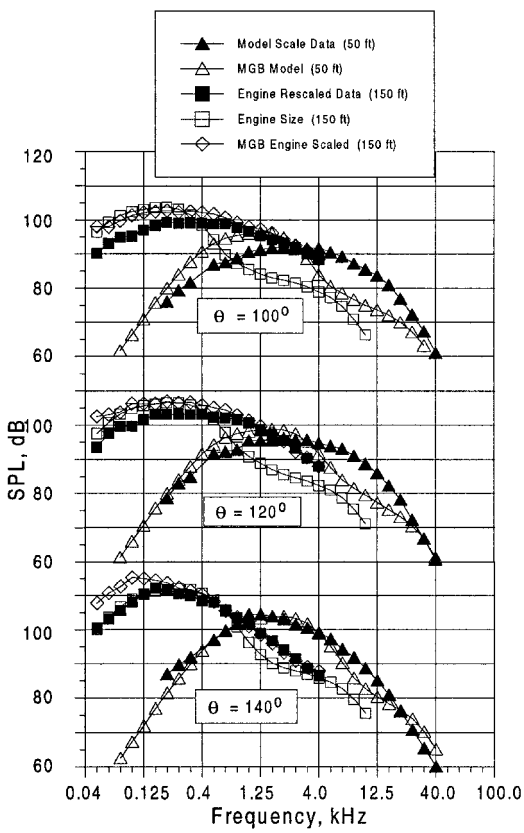

Fig. 10 Engine scaled splitter one-third octave spectra comparisons at 150-ft distance.

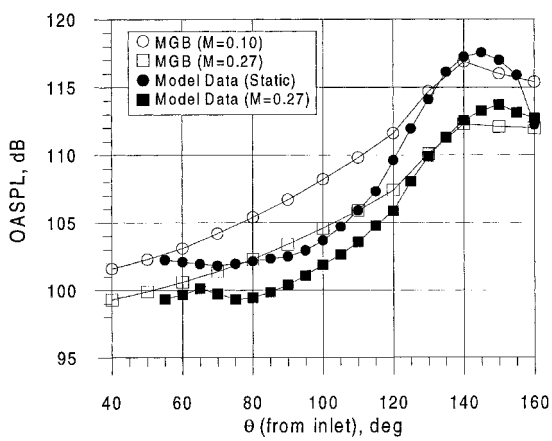

Fig. 11 Forward-flight effect on OASPL for model scale splitter at 50-ft distance.

conditions of $M_\infty = 0.1$, where aerodynamic (*LV*) data were obtained. MGB calculations are shown in Fig. 11. The OASPL predictions confirm experimental observations and show the expected increase in OASPL levels with decreased flight Mach number.

Forced Mixer Studies

Three-dimensional calculations for 12- and 20-lobed mixer nozzles have been performed using the initialization procedures cited in the preceding text. The three-dimensional CFD flowfield solution was then adapted to the axisymmetric MGB analysis. An equivalent axisymmetric flowfield was developed by circumferentially mass-averaging the three-dimensional flowfield in the manner suggested by Mani et al.[3] This approach was assumed adequate because the NASTAR predictions indicate that the flowfield rapidly approaches an axisymmetric pattern in the external plume. OASPL spectra comparisons with experimental data for the 12- and 20-lobed mixer nozzles are shown in Fig. 12. While the analysis is in general agreement with the data, the analysis incorrectly predicts a higher noise level for the 20-lobed mixer nozzle.

A closer look at the axisymmetric-averaging approach is now presented. Figure 13 coplots the axisymmetric splitter velocity profile with the circumferentially averaged 12- and 20-lobed mixer velocity profiles. The mixer nozzles (both 12- and 20-lobed) reduce the peak velocity from 1500 to 1100 fps; however, the 20-lobed mixer has a higher velocity level inboard of the peak. This helps explain the anomalous MGB noise prediction results shown in Fig. 12. A closer look at the exit plane velocity field for both mixer nozzles is shown in Fig. 14. Clearly, the 12-lobed nozzle has peak velocities in excess of 1300 fps, whereas the 20-lobed nozzle's peak velocity is less than 1200 fps. The linear-averaging process therefore produces the erroneous profiles seen in Fig. 13. In hindsight, an averaging procedure that weights the velocity nonlinearly like the Lighthill theory is most likely necessary.

Additional insight to the mixing/noise generation process can be gained by examining the internal and external k field. Equation (4) indicates that the noise source intensity is dependent on k; i.e., higher k produces more noise. From the exit plane contours shown on Fig. 15, maximum values of k are produced by the shear layers along the lobe sidewalls (linear averaging would not account for this), and are much larger than generated by the splitter. On the other hand, Fig. 16 indicates that the largest k regions occur in the exhaust plume and that the splitter and mixer nozzles appear to have the same k levels. The vertical scale in Fig. 16 has been enlarged by a factor of 2 to improve the display. Although the nozzle wall is not displayed, the splitter and nozzle wall shear layers are clearly visible. In the crest-cut mixer view shown in Fig. 16, only the nozzle shear layer is seen. Both configurations, however, have relatively the same turbulence intensity in the external plume.

Finally, by displaying the axial contribution to OASPL for a given viewing angle (Fig. 17), one can examine the cumulative noise contribution at the 120-deg viewing angle for the axisymmetric splitter and the 12-lobed mixer. Because the three-dimensional mixer calculation was somewhat limited, a restarted, axisymmetric-extended domain calculation was performed and is also displayed. First, one can verify Goldstein's observation that the majority of the noise occurs within 10 nozzle diameters of the exit plane for axisymmetric jets. Furthermore, one can see that the improved mixedness of the lobed mixer flow produces little additional noise downstream of the exit plane.

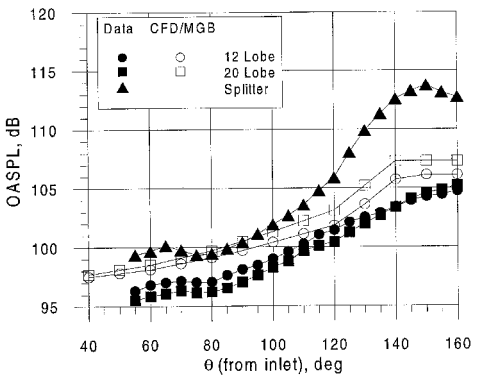

Fig. 12 MGB/data comparisons of OASPL for 12- and 20-lobed mixer nozzles at 50-ft distance.

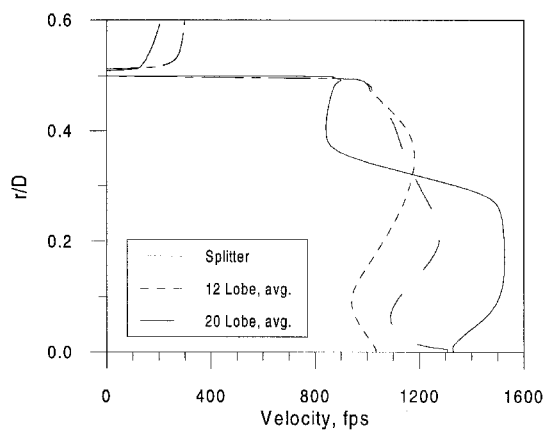

Fig. 13 Circumferentially mass-averaged exit plane axial velocity profiles for splitter, 12-, and 20-lobed nozzles.

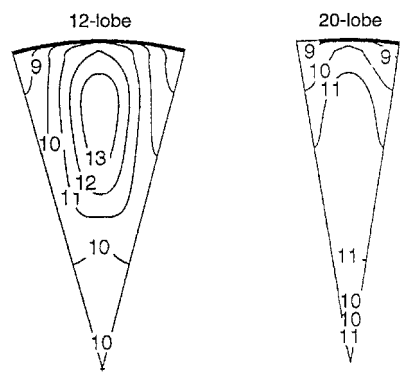

Fig. 14 Exit plane velocity field for 12- and 20-lobed mixer nozzles ($U \times 10^{-2}$ fps).

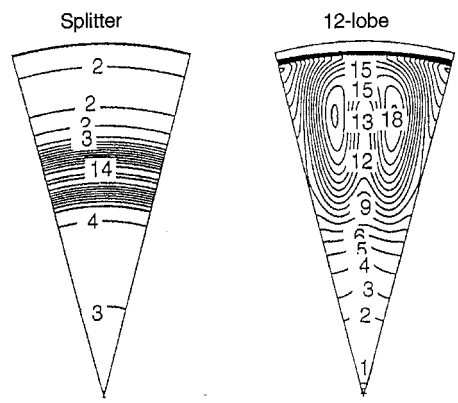

Fig. 15 Exit plane turbulent kinetic energy contours for axisymmetric splitter and 12-lobed mixer nozzles ($k \times 10^{-3}$, ft²/s²).

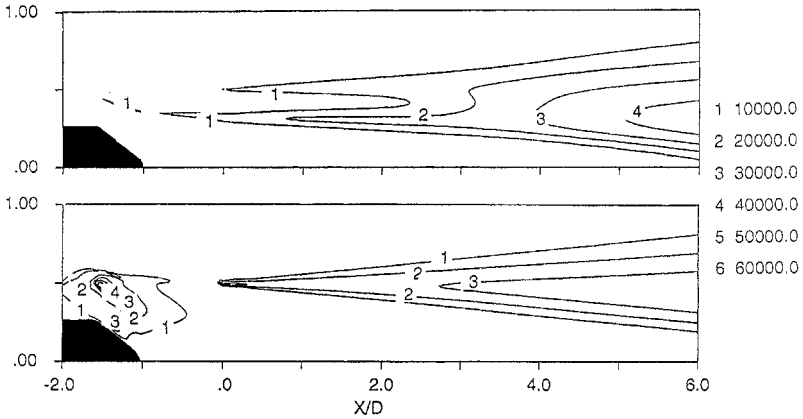

Fig. 16 Axial view of turbulent kinetic energy contours in the exhaust of an axisymmetric splitter and 20-lobed mixer nozzles ($k \times 10^{-4}$, ft^2/s^2).

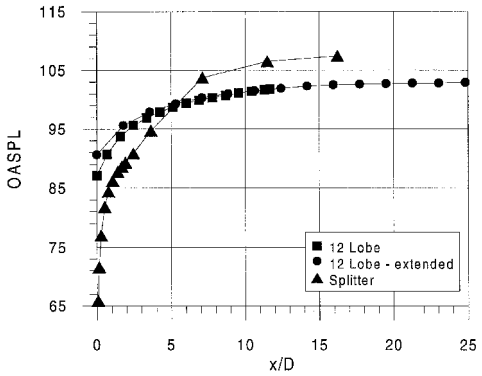

Fig. 17 Calculated axial contribution of OASPL for axisymmetric splitter and 12-lobed mixer nozzles.

Concluding Remarks

The MGB analysis, in conjunction with a state-of-the-art Navier–Stokes flow solver, has been successfully applied to predict the acoustic characteristics of a multistream axisymmetric nozzle. From these calculations, note that 1) MGB provides reasonable acoustical signature predictions for axisymmetric multistream nozzles, 2) MGB provides reasonable acoustical signature predictions of scaling effects, e.g., size and observer distance, and 3) MGB is a useful analytical tool for assessing turbulence modeling and input boundary condition effects, and that sensitivities of order 2–4 dB were noted.

While calibrations with experimental data were good, it is believed that the CFD/MGB analysis approach is best suited for predicting qualitative trends rather than absolute levels.

Similar comparisons performed for three-dimensional forced mixer nozzles were less successful. While the analyses predicted the general shift in directivity pattern from the axisymmetric splitter nozzle, they were unable to successfully discriminate between different lobed mixer configurations. This appears to be largely because of the inability of the circumferential-averaging procedure to represent the three-dimensional problem, rather than the accuracy limitations of the CFD analysis.

Acknowledgments

This work was supported by a Task Order Contract NAS3-26618 from the NASA Lewis Research Center. The authors would like to thank Abbas Khavaran of NYMA for his assistance in the modification and application and of his modified MGB code for use in this effort. The authors also thank James Bridges of NASA Lewis Research Center for his support in providing the experimental data used in this study.

References

[1]Rhie, C. M., and Chow, W. L., "Numerical Study of the Turbulent Flow Past and Airfoil with Trailing Edge Separation," *AIAA Journal*, Vol. 21, No. 11, 1983, pp. 1525–1532.

[2]Malecki, R., Mityas, S., and Lord, W., "Navier-Stokes Analysis of an Ejector and Mixer-Ejector Operating at Pressure Ratios in the Range 2–4," AIAA Paper 90-2730, July 1990.

[3]Mani, R., Balsa, T. E., Gliebe, P. R., Kantola, R. A., Stringes, E. J., and Wang, J. F. C., "High Velocity Jet Noise Source Location and Reduction: Task 2-Theoretical Developments and Basic Experiments," Federal Aviation Administration, RD-76-79-II, May 1978.

[4]Patankar, S. V., *Numerical Heat Transfer and Fluid Flow*, Hemisphere, New York, 1980.

[5]Jones, W. P., and Launder, B. E., "The Prediction of Laminarization with a Two-Equation Model of Turbulence," *International Journal of Heat and Mass Transfer*, Vol. 15, No. 2, 1972, pp. 301

[6]Khavaran, A., Krejsa, E. A., and Kim, C. M., "Computation of Supersonic Jet Mixing Noise for an Axisymmetric CD Nozzle Using k-ε Turbulence Model," AIAA Paper 92-0500, Jan. 1992.

[7]Khavaran, A., Krejsa, E. A., and Kim, C. M., "Computation of Supersonic Jet Mixing Noise for an Axisymmetric CD Nozzle," *Journal of Aircraft*, Vol. 31, No. 3, 1994, pp. 603–609.

[8]Zysman, S. H., Chiappetta, L. M., Saiyed, N. H., and Podboy, G. G., "Flowfield Measurements and Analysis of a 1/7-Scale Mixed Flow Exhaust System Model," AIAA Paper 95-2744, July 1995.

[9]Podboy, G. G., Bridges, J., Saiyed, N. H., and Krupar, M., "Laser Doppler Velocimeter System for Subsonic Jet Mixer Nozzle Testing at the NASA Lewis Aeroacoustic Propulsion Lab," AIAA Paper 95-2787, July 1995.

[10]Dannenhoffer, J. F., III, "Computer-Aided Block-Structuring Through the Use of Optimization and Expert System Techniques," AIAA Paper 91-1585, June 1991.

[11]Dannenhoffer, J. F., III, "A Block-Structuring Technique for General Geometries," AIAA Paper 91-0145, Jan. 1991.

[12]Sarkar, S., Erlebacher, G., Hussaini, M. Y., and Kreiss, H. O., "The Analysis and Modeling of Dilatational Terms in Compressible Turbulence," *Journal of Fluid Mechanics*, Vol. 227, 1991, pp. 473–493.

[13]Choi, D., Weeratunga, S., and Knight, C. J., "A Numerical Method for Navier-Stokes Equations with Finite Rate Chemistry," AIAA Paper 89-1857, June 1989.

[14]Yamamoto, K., Brausch, J. F., Balsa, T. F., Janardan, B. A., and Knott, P. R., "Experimental Investigation of Shock-Cell Noise Reduction for Single Stream Nozzles in Simulated Flight, Comprehensive Data Report, Vols. 1–3," NASA CR-168234, 1984.

[15]Choi, D., Sabnis, J. S., and Barber, T. J., "Application of an RNG k-ε Model to Compressible Turbulent Shear Layers," United Technologies Research Center, Rept. 93-25, June 1993; also AIAA Paper 94-0188, Jan. 1994.

[16]Soderman, P. T., "On the Scaling of Small-Scale Jet Noise to Large Scale," *Proceedings of the DGLR/AIAA 14th Aeroacoustics Conference* (Aachen, Germany), AIAA, Washington, DC, 1992, pp. 663–671.

[17]Simonich, J., "Hush Kit Directional Microphone Acoustic Test," United Technologies Research Center, Rept. 90-30, Aug. 1990.